

An Experimental Investigation of Airfoil Tonal Noise Caused by an Acoustic Feedback Loop

Elias J. G. Arcondoulis, Con J. Doolan, Anthony C. Zander and Laura A. Brooks

School of Mechanical Engineering, The University of Adelaide, Adelaide, Australia

ABSTRACT

Airfoils in low-to-moderate Reynolds number flows produce discrete tones which can be annoying to the human ear and potentially impede the design of fans, compressors, helicopter rotors and unmanned air vehicles. This paper discusses an experimental investigation into the generation of tones from a NACA 0012 airfoil for varying angles of attack and Reynolds numbers between 50,000 and 150,000. The investigator employed acoustic beamforming, hot-wire anemometry, single microphone measurements and surface flow visualisation techniques. The experimental results were used to calculate flow and noise parameters that were used in an acoustic feedback loop model to determine its validity. Surface flow visualisation techniques revealed locations of boundary layer separation. The phase difference between the noise signal and local flow velocities near the airfoil surface was used to measure the convective velocity of the disturbances in the airfoil boundary layer. A good agreement between the experiment and predicted tonal frequencies was obtained when the experimentally determined length and velocity scales were used in the feedback model, supporting the applicability of a feedback model for tonal noise in this case.

INTRODUCTION

The mechanisms that generate discrete tones from airfoils in low-to-moderate Reynolds number flow conditions have been under scrutiny since Paterson et al. (1973) suggested that the tonal noise was caused by a vortex shedding process. Since this time a general consensus for the generation of this tonal noise has not been achieved in the scientific community.

Tam (1974) pioneered the concept of an acoustic feedback mechanism, suggesting that the amplification of noise caused by a diffraction process at the trailing edge (Ffowcs Williams and Hall, 1970) was due to an acoustic feedback loop between the trailing edge and the location of wake vibrations in the wake region. However, Tam and Ju (2011) recently showed using computational techniques that a feedback loop does not exist at zero angle of attack and that facility effects are responsible for the generation of secondary tones. Lawson et al. (1994) and Nash et al. (1998) suggest that an acoustic feedback mechanism is not necessary to observe tonal noise. Using flow visualisation techniques they show that a separated flow region near the trailing edge forms vortices, which are then shed downstream of the trailing edge, resulting in tonal noise generation. Desquesnes et al. (2007) proposed that an acoustic feedback loop exists between the noise source location near the trailing edge and a separation bubble on the airfoil pressure surface, as depicted in Figure 1.

Arbey and Bataille (1983) suggested that a feedback mechanism involves diffraction at the trailing edge, causing out-of-phase acoustic waves to radiate upstream to the point of maximum flow velocity on the airfoil as depicted in Figure 2. This paper details a comparison of acoustic feedback loop lengths by inputting experimentally obtained flow and noise parameters into a feedback model proposed by Arbey and Bataille (1983):

$$\frac{f_n L}{C_r} \left(1 + \frac{C_r}{C_0 - U} \right) = n + \frac{1}{2} \quad (1)$$

where f_n represents the tone frequency (Hz) as a function of n , C_r is the convection flow velocity (m/s), C_0 is the speed of sound (m/s), U is the free-stream flow speed (m/s) and n is a positive integer representing the number of convective wavelengths.

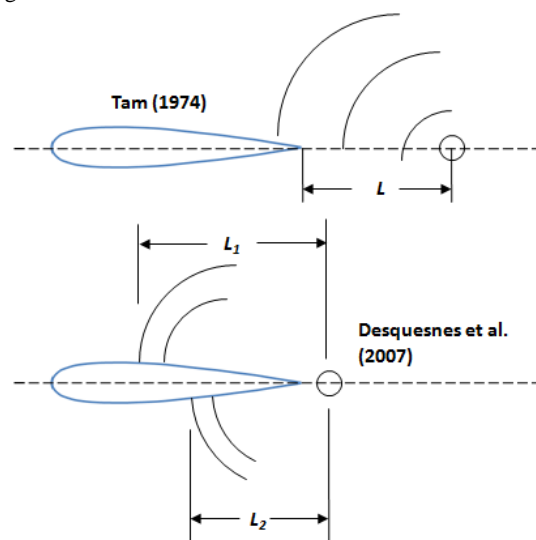


Figure 1. Schematic diagram of acoustic feedback models, proposed by Tam (1974) and Desquesnes et al. (2007). The open circle depicts the noise source location, L represents a feedback loop length and L_1 and L_2 represent two loops on the airfoil suction and pressure sides, respectively.

The acoustic feedback models discussed possess a common structure; an acoustic wave radiates upstream from its source and becomes positively reinforced at some point along the airfoil chord. These models imply that the location of the start and closing points of the feedback loop are independent of the Reynolds number. They also assume that the convective velocity of the disturbances in the flow within the boundary layer is independent of angle of attack and Reynolds number.

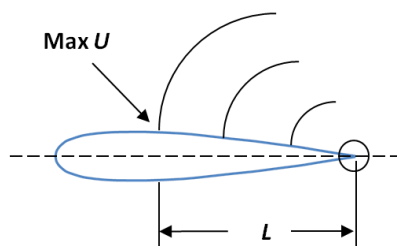


Figure 2. Schematic diagram of an acoustic feedback model, proposed by Arbey and Bataille (1983). The open circle depicts the noise source location, and L is the distance between the point of maximum flow velocity ($Max U$) and the trailing edge.

EXPERIMENTAL FACILITY

Experimental measurements were obtained in an Anechoic Wind Tunnel (AWT), located in the Sir Edmond Holden Laboratory at The University of Adelaide, South Australia. This is a low-speed wind tunnel, designed for scale model testing, situated within an anechoic room that is approximately $1.4\text{ m} \times 1.4\text{ m} \times 1.6\text{ m}$. The walls are acoustically treated with foam wedges. The contraction outlet (test section) has a working area of 75 mm (height) \times 275 mm (width).

A NACA 0012 airfoil section was used for the results presented in this paper. The airfoil has a chord of 67 mm and a span of 275 mm , which is the same width as the working section as shown in Figure 3.

Background Noise

A measurement of background noise (including the airfoil housing) with varying airflow speeds in the AWT was recorded using a B&K 1/2" microphone (Model No. 4190), directly above the airfoil trailing edge location. Data were obtained for five seconds with a sampling rate of 2^{15} Hz . The frequency resolution of the processed spectra was 1 Hz .

The flow velocities 11.3 m/s , 22.5 m/s and 33.8 m/s correspond to the flow speeds required to achieve Reynolds numbers of $50,000$, $100,000$ and $150,000$ respectively for the 67 mm chord airfoil used in this study. As later shown in the paper, the minimum investigated frequency is 500 Hz . The maximum background noise due to flow at 33.8 m/s without the airfoil present is approximately 28 dB (ref $20 \times 10^{-6}\text{ Pa}$) at 540 Hz .

EXPERIMENTAL PROCEDURES

Acoustic Beamforming

An acoustic beamformer, shown in Figure 4, was designed and manufactured for aeroacoustic experiments in the AWT, to identify airfoil noise source locations. The array contains 63 Lectret microphones, arranged in a modified logarithmic spiral, which is discussed in detail in Arcondoulis et al. (2011). The array covers an approximate area of $700\text{ mm} \times 700\text{ mm}$ and is positioned in a horizontal plane 620 mm in the vertical direction above the centreline of the working section. The centre microphone of the array is directly above the airfoil trailing edge.

The data acquisition (DAQ) system used for the acoustic beamforming tests was a National Instruments (NI) PXI-1042Q Chassis, with four PXI-4496 DAQ cards. Each card contains 16 channels, thus allowing up to 64 channels of real-time data.

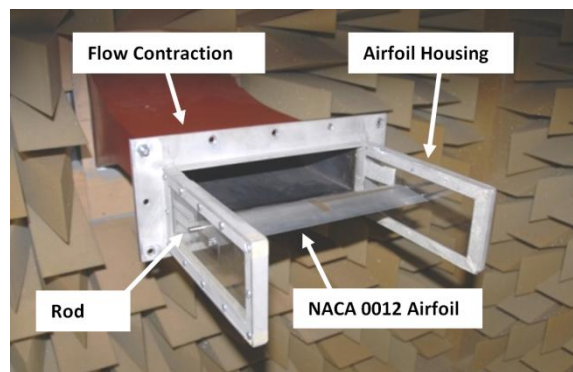


Figure 3. NACA 0012 airfoil secured to the AWT contraction.



Figure 4. Acoustic beamformer array installed in the AWT.

A MATLAB DAQ interface was used to collect these data at a sampling frequency of 2^{15} Hz for five seconds. The data to be acquired were band-pass filtered between 50 Hz and 10 kHz and passed through a Fast Fourier Transform (FFT) algorithm. The data were converted into a cross-spectral matrix, which contains the products of the complex pressure spectra of all microphones multiplied by their conjugates. The autospectra were removed and the complex pressures were passed into a cross-spectral beamforming algorithm. A DAMAS beamforming algorithm was used to further resolve the acoustic sources (Brooks and Humphreys, 2006).

The acoustic source was resolved over a scanning grid containing 51×51 lines (2601 points) over a $500\text{ mm} \times 500\text{ mm}$ area, containing an aerial view of the airfoil. 5000 iterations of a DAMAS solution scheme (presented by Brooks and Humphreys, 2006) were performed.

The refraction effect of the tonal noise passing through half of the AWT jet was approximated, using a method presented by Amiet (1977). To reduce computational time, a shear layer correction was not performed at every scanning grid point within the beamforming algorithm, but was calculated assuming the noise radiated at 90° relative to the direction of the flow. The amount of refraction experienced at that location was applied to every scanning grid point. In Arcondoulis et al. (2012) it was shown that the greatest error of this approximation is less than 0.1 mm at the upper and lower bounds of the scanning grid. The approximation method used is discussed in detail in Arcondoulis et al. (2012).

Hot-wire Anemometry and Single Microphone Tests

To measure the local flow conditions around the airfoil profile, a hot-wire probe was attached to an arm connected to a traverse. A flow measurement was obtained using the hot-wire probe and then moved using an automated computer script via the traverse to take another measurement. An example of a hot-wire anemometry test in the AWT is shown in Figure 5.

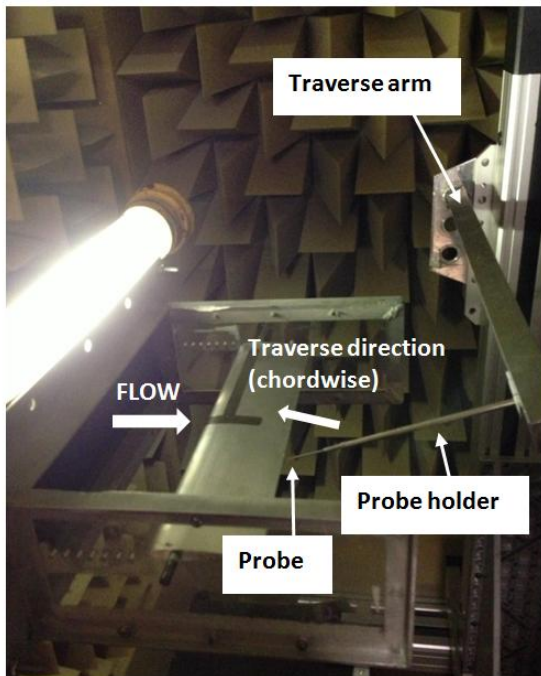


Figure 5. Hot-wire probe connected to the traverse arm in the AWT for flow measurements.

The software package Thermalpro was used to interface the probes and the PC. The probes were powered using an IFA300 TSI constant temperature anemometer box.

The hot-wire probe was calibrated by measuring the voltage from the probe resistance against a known compressed air pressure source. A range of pressures were used to fit a calibration curve, due to the non-linear behaviour of the probe.

The noise spectra were obtained simultaneously with the hot-wire measurements, using a MATLAB script which triggered the DAQ for both channels simultaneously. The microphone used was a B&K 1/2" microphone (Model No. 4190) and was placed 620 mm directly above the airfoil trailing edge. The data were collected at a sampling frequency of 2^{15} Hz for five seconds and are presented with a frequency resolution of 1 Hz. The microphone was calibrated using a 1 kHz tone piston-phon.

Surface Flow Visualisation

A mixture of linseed oil and talcum powder (Arcondoulis et al., 2013) was spread across a segment of a NACA 0012 airfoil on the pressure and suction airfoil surfaces. This was done to identify locations of boundary layer separation and shear layer reattachment.

For each flow visualisation, images were captured using a camera at the top of the airfoil housing, aimed at the airfoil surface. Flow separation and reattachment locations were estimated by identifying the locations where the oil mixture transitioned from attached to removed from the airfoil surface. These locations were measured on each photograph and scaled relative to the airfoil chord length and converted into physical distances.

Test Conditions

The airfoil was placed at three geometric angles of attack during testing, 0° , 5° and 10° . Since the AWT jet height is finite, two-dimensional correction factors were applied to determine the true effect of the airfoil angle of attack (Brooks et al. 1989). Applying a correction factor to a 67 mm airfoil chord and a 75 mm jet height in accordance with Brooks et al. (1989), the corrected angles of attack were less than the true, geometric angles of attack. The actual angles of attack, α , are corrected as 0° is 0° (true), 5° (geometric) is 1.58° (true) and 10° (geometric) is 3.16° (true). Throughout the remainder of this paper, only the true angle of attack will be stated.

Acoustic beamforming, hot-wire anemometry, single microphone measurements and surface flow visualisation were performed for Reynolds numbers, $Re = 50,000, 100,000$ and $150,000$. At each Reynolds number, measurements were obtained at angles of attack, $\alpha = 0^\circ, \pm 1.58^\circ$ and $\pm 3.16^\circ$.

EXPERIMENTAL RESULTS

Noise Spectra

The noise spectra of a NACA 0012 airfoil in Reynolds number flows of 50,000 to 150,000 were obtained using a single microphone. The noise spectra at $Re = 100,000$ and $\alpha = 0^\circ$ is presented in Figure 6.

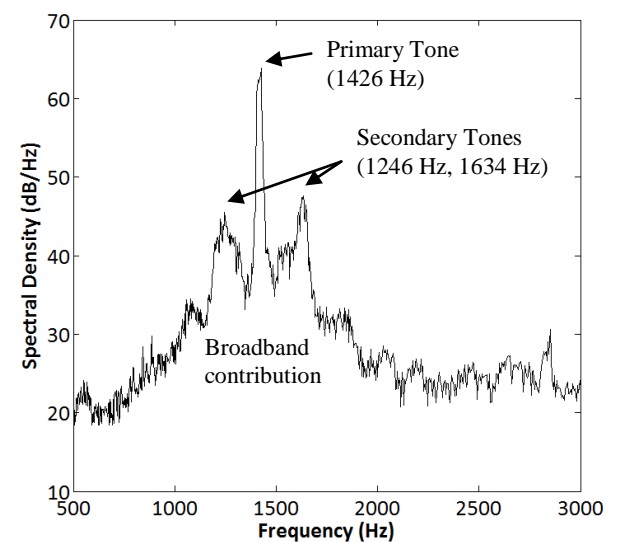


Figure 6. Noise spectrum of a NACA 0012 airfoil at $Re = 100,000$ and $\alpha = 0^\circ$. The primary and secondary tones are identified on the figure. The broadband contribution region is shown on the figure.

There is a distinct primary tone, which is greater than 30 dB in magnitude relative to the broadband contribution. There also exist secondary tones, which are greater than 10 dB relative to the broadband contribution. In each of the flow cases investigated, the primary tone has a smaller bandwidth (measured 3 dB from the peak) than the secondary tones.

For all Reynolds numbers considered, tones were observed for $\alpha = 0^\circ$ and 1.58° . The primary and secondary tones observed at these angles of attack are listed in Table 1 and Table 2 respectively. No tones were recorded at $\alpha = 3.16^\circ$; only a broadband contribution was observed above the background noise.

Table 1. Primary tone frequencies for angles of attack, 0° and ±1.58°.

Reynolds Number	Primary Tone Frequency (Hz)	
	0°	±1.58°
50,000	588	605
100,000	1426	1471
150,000	2039	2904

Table 2. Secondary tone frequencies for angles of attack, 0° and ±1.58°.

Reynolds Number	Secondary Tone Frequencies (Hz)	
	0°	±1.58°
50,000	494, 670	514, 701
100,000	1246, 1634	1714
150,000	1714, 2362, 2783, 3108	2678, 3377

Noise Source Location

A DAMAS beamformer image for a tone at 1426 Hz at Re = 100,000 and $\alpha = 0^\circ$ is presented in Figure 7. The maximum source strength is shown to be located on the airfoil trailing edge. This result was typical for all Reynolds numbers and angles of attack considered in this study.

The source is shown to be concentrated at the centre of the airfoil span. It is likely that this is due to the sources along the airfoil span producing coherent noise which is detected by the beamformer as a single source located at the spanwise centre. The coherence of tonal noise sources along the span does not impact the ability of the beamformer to resolve the acoustic source location in the chordwise direction, which is of greater importance for acoustic feedback loop analysis.

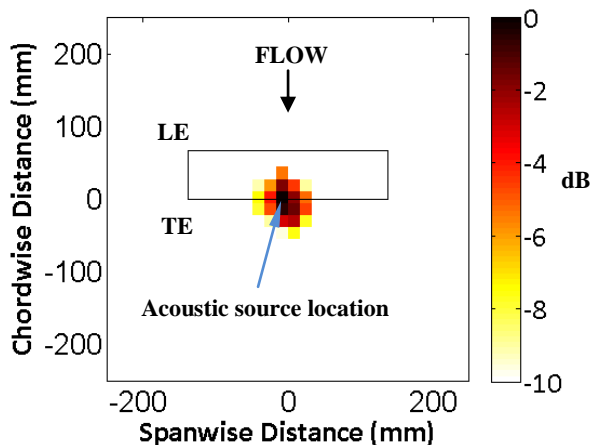


Figure 7. DAMAS beamformer output for a NACA 0012 airfoil at Re = 100,000 and $\alpha = 0^\circ$. LE and TE denote leading and trailing edge, respectively. The legend represents amplitude in dB, normalised to the maximum acoustic source strength.

Flow Measurements

Flow measurements were obtained using hot-wire anemometry at a fixed distance of 1 mm above the airfoil surface. Mean velocity flow measurements were obtained in 1 mm increments in the chordwise direction, from the trailing edge to the leading edge, following the NACA 0012 airfoil profile. This was performed for all angles of attack and Reynolds numbers considered in this paper. An example mean velocity plot around the airfoil surface is shown in Figure 8 for Re = 100,000 and $\alpha = 0^\circ$. The maximum mean velocity is identified on the figure.

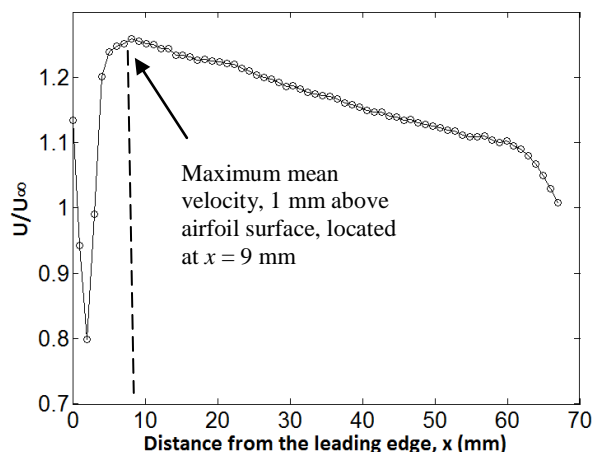


Figure 8. Mean flow velocity measured 1 mm above the airfoil surface, from the leading edge ($x = 0$ mm) to the trailing edge ($x = C = 67$ mm) at Re = 100,000 and $\alpha = 0^\circ$. The mean velocity, U , is normalised to the freestream velocity, $U_\infty = 22.54$ m/s. The location of the maximum mean velocity is identified on the figure.

A comparison of mean velocity plots between the experimental data and XFOIL (Drela, 1989), a widely used software program that employs the panel method to solve potential, viscous flows of airfoils, was performed.

At zero angle of attack, both XFOIL and experiments showed that the point of maximum mean velocity was located 9 mm from the leading edge for Re = 100,000 and 150,000. At Re = 50,000, experiments showed that the point of maximum mean velocity was 23 mm from the leading edge and XFOIL predicted 9 mm from the leading edge. This difference may be explained by the height of the probe from the airfoil surface being within the boundary layer and thus not measuring the maximum mean airfoil velocity.

For all Reynolds numbers investigated at $\alpha = 1.58^\circ$, the point of maximum mean velocity calculated using XFOIL and measured experimentally were both 4 mm from the leading edge on the airfoil pressure side. These matching results provided confidence in the experimental measurements.

The points of maximum mean velocity obtained via experiment are listed in Table 3. The mean flow measurements obtained via experiment are presented in Figure 9. These plots show the differences in the point of maximum mean velocity for each angle of attack and Reynolds number flow condition. At higher angles of attack, the point of maximum mean velocity is shown to move further upstream on the pressure side whereas it moves further downstream on the suction side, as expected from potential flow theory.

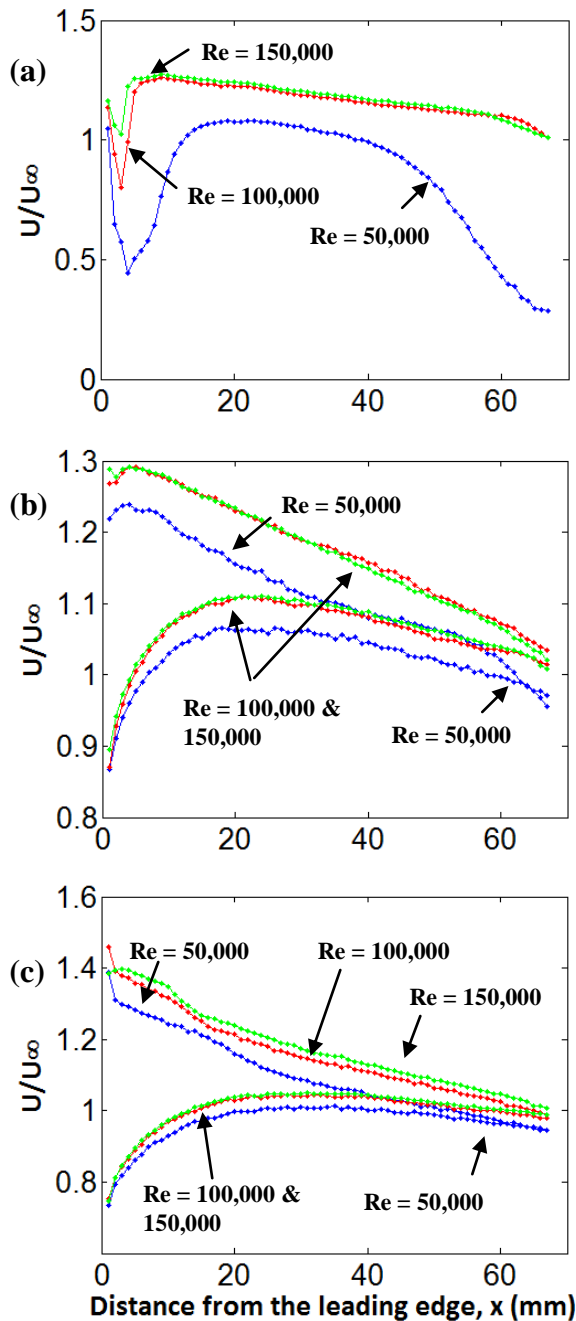


Figure 9. Mean flow velocity measurements, obtained 1 mm above the airfoil profile, from the leading edge to the trailing edge of a NACA 0012 airfoil with 67 mm chord at (a) 0° angle of attack, (b) ±1.58° angle of attack and (c) ±3.16° angle of attack. The pressure side curves are the upper part of each of (b) and (c), the suction side curves are in the lower part.

At $\alpha = 3.16^\circ$, the suction and pressure side curves meet at the trailing edge, which is to be expected for all Reynolds number flows. However, this was not the case for the $\alpha = 1.58^\circ$ measurements. It is unknown why this occurred. The agreement between the points of maximum mean velocity with the measured and XFOIL values at $\alpha = 1.58^\circ$, however, provides confidence that the points of maximum mean velocity measured via experiment are accurate. The mean velocity values near the trailing edge are not used in the analyses presented

in this paper and therefore should have little bearing on the outcome of the validity of a proposed acoustic feedback model.

Table 3. Point of maximum mean velocity 1 mm above the airfoil surface from the leading edge. The stated angles are angles of attack.

Reynolds Number	Maximum mean velocity location from the leading edge (mm)				
	0°	1.58°	-1.58°	3.16°	-3.16°
50,000	23	4	26	0	35
100,000	9	4	22	0	28
150,000	9	4	24	2	31

Flow Separation and Reattachment Locations

The flow forced the oil mixture downstream from the leading edge to the point of flow separation. For the flow condition of $Re = 100,000$ and $\alpha = 0^\circ$, the oil mixture collected 40 mm downstream of the leading edge, which represents the point of flow separation, S, as identified in Figure 10. Near the trailing edge, the mixture was removed from the airfoil surface, which represents a point of flow reattachment, as labelled R. This occurred 3 mm from the trailing edge (64 mm from the leading edge).

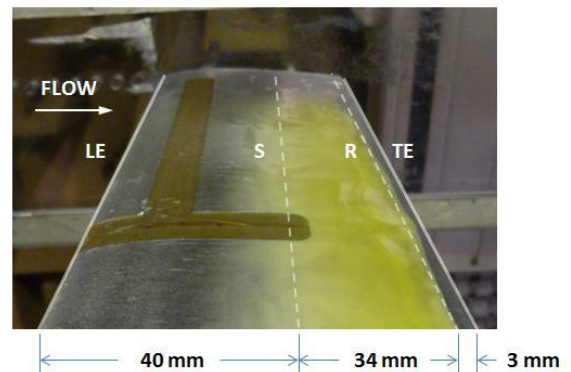


Figure 10. Photo of the oil mixture pattern showing surface flow behaviour. The pattern is shown for a NACA 0012 airfoil, at $Re = 150,000$ and $\alpha = 0^\circ$. LE, TE, S and R denote Leading Edge, Trailing Edge, Separation and Reattachment, respectively.

Surface flow visualisation tests performed on the pressure side at $\alpha = 1.58^\circ$ and 3.16° showed boundary layer separation further from the leading edge for the same Reynolds number flow than at $\alpha = 0^\circ$, with the $Re = 50,000$ flow being an exception. On the suction side, separation occurred rapidly after the leading edge and flow reattachment was observed further downstream, creating a mid-chord separation bubble.

Example surface flow visualisation cases are presented in Figure 11, which shows patterns for the flow conditions of $Re = 150,000$, $\alpha = 1.58^\circ$ on the suction side and $Re = 150,000$, $\alpha = 3.16^\circ$ on the pressure side respectively. For the purposes of feedback loop analysis, the points of boundary layer separation relative to the leading edge are provided in Table 4.

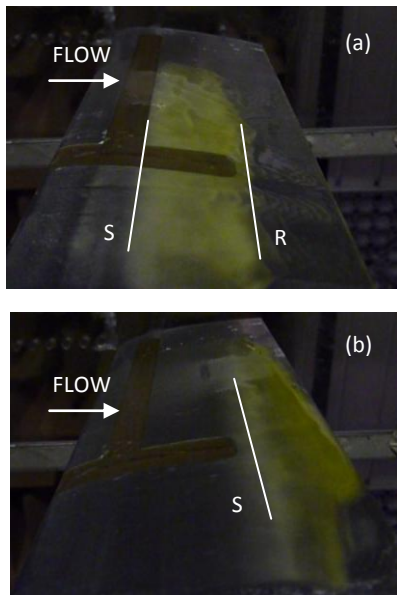


Figure 11. Photo of the oil mixture pattern showing surface flow behaviour for a NACA 0012 airfoil. (a) $Re = 150,000$, $\alpha = 1.58^\circ$ on the suction side. (b) $Re = 150,000$, $\alpha = 3.16^\circ$ on the pressure side. S and R denote Separation and Reattachment, respectively.

Table 4. Point of boundary layer separation from the airfoil surface, from the leading edge. A positive angle of attack represents the airfoil pressure side; a negative angle represents the airfoil suction side.

Reynolds Number	Boundary layer separation from the leading edge (mm)				
	0°	1.58°	-1.58°	3.16°	-3.16°
50,000	22	13	5	12	2
100,000	29	30	10	37	2
150,000	40	44	21	52	2

Convective Disturbance Velocity

To calculate the convective disturbance velocity near the airfoil surface, the phase difference between the flow and noise signals was obtained. A spectrogram output of the phase difference between the flow and noise signals at $Re = 100,000$ and $\alpha = 0^\circ$ is presented in Figure 12. A convective disturbance wavelength can be identified as a complete change of phase between the flow and noise signals. A typical wavelength is identified in Figure 12a.

The convective disturbance wavelength, λ (mm), is calculated by measuring the distance between the peaks of the spectrogram plot, for the corresponding tone frequency. The convective disturbance velocity is calculated by

$$C_r = f\lambda \tag{2}$$

where f is the tone frequency in Hz. An example calculation is performed using data collected at $Re = 100,000$ and $\alpha = 0^\circ$ for a primary tone frequency of 1426 Hz, shown in Figure 12b. Using the first three peaks at 1 mm, 7 mm and 13 mm,

they are each separated by 6 mm, thus $\lambda = 6$ mm. The primary tone frequency is 1426 Hz and using Equation 2 yields $C_r = 1426 \times 6/1000 = 8.56$ m/s. The convective disturbance velocity is often presented in ratio form relative to the freestream velocity, which is $C_r / U_\infty = 8.56/22.54 = 0.38$.

The convective disturbance velocity ratio was also calculated for $\alpha = 1.58^\circ$ and $Re = 50,000, 100,000$ and $150,000$, using the primary tone frequencies, presented in Table 5. The convective disturbance velocity ratio was found to be the same whether a primary or secondary tone was used for its evaluation. The convective disturbance velocity ratio was not computed at $\alpha = 3.16^\circ$ as there were no distinct tones in the measured noise and thus no visible wavelengths in the spectrogram outputs.

Table 5. Convective disturbance velocity ratio, C_r / U_∞ , for angles of attack, 0° and $\pm 1.58^\circ$, calculated using the primary tone frequencies presented in Table 1.

Reynolds Number	C_r / U_∞	
	0°	$\pm 1.58^\circ$
50,000	0.32	0.46
100,000	0.38	0.46
150,000	0.42	0.40

FEEDBACK LOOP ANALYSIS

The boundary layer separation length, L , was used to investigate the validity of Arbey and Bataille’s (1983) feedback loop model. Their equation was rearranged as

$$f_n = \frac{C_r}{L} (n + 0.5) \left(1 + \frac{C_r}{C_0 - U} \right)^{-1} \tag{3}$$

Previous work (Tam, 1974; Arbey and Bataille, 1983; Desquesnes et al., 2007) used constant values of L and C_r for all U and α . However as shown via experiment, C_r varies with U and α for a NACA 0012 airfoil and thus cannot be considered a constant in the feedback model. By considering the trailing edge as the start of the feedback loop and the point of flow separation as the closing point of the feedback loop, then the feedback loop length, L , also varies with U and α , as the point of flow separation is flow dependent. These feedback lengths are provided in Table 6. Tables 7 and 8 list the results of using the boundary layer separation feedback length in Equation 3 and the comparison with the experimentally measured tones for $\alpha = 0^\circ$ and 1.58° respectively.

Table 6. Feedback lengths, L (mm), at $\alpha = 0^\circ$ and 1.58° . These lengths are the distance from the point of interest to the trailing edge.

Reynolds Number	$\alpha = 0^\circ$		$\alpha = 1.58^\circ$	
	Max. U	BL Sep ⁿ	Max. U	BL Sep ⁿ
50,000	44	45	63	54
100,000	58	38	63	37
150,000	58	27	63	23

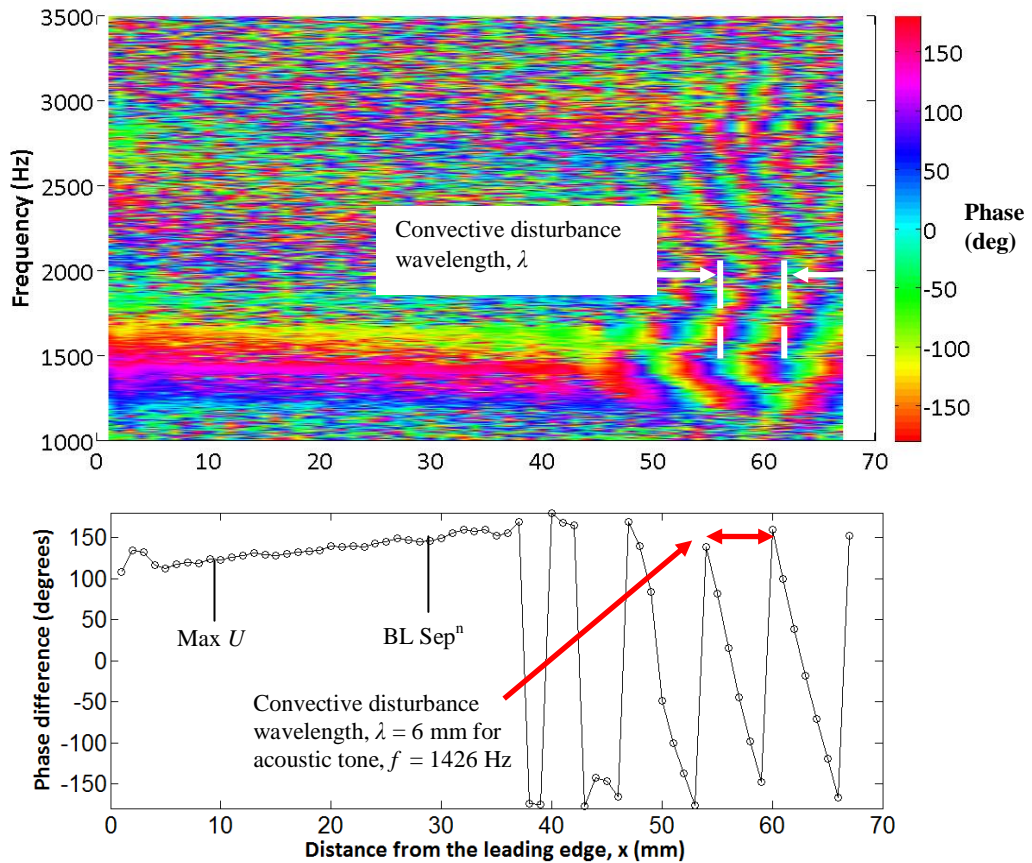


Figure 12. (a) Spectrogram of the phase difference (degrees) between the flow and noise signals for frequencies 1000 Hz to 3500 Hz, which contains all of the measured tones at $Re = 100,000$, $\alpha = 0^\circ$. (b) Phase difference between the flow and noise signals at a tone of frequency 1426 Hz. Flow measurements were obtained 1 mm above the airfoil surface in 1 mm chordwise increments from the leading edge ($x = 1$ mm) to the trailing edge ($x = 67$ mm). Acoustic measurements were obtained 620 mm directly above the airfoil trailing edge. A convective disturbance wavelength is identified on the figure.

Table 7. Feedback analysis at $\alpha = 0^\circ$, using the boundary layer separation feedback length, L . The predicted tones (Hz) using a feedback model are shown and the experimentally measured tones are presented in brackets. The relative error of the predicted to the experimentally measured tones is also presented. The primary tone is presented in bold case.

Re $\times 10^3$	n					
	3	4	5	6	7	8
50				515 (494) 4%	595 (588) 1%	674 (670) 1%
			1207 (1246) 3%	1427 (1426) <1%	1646 (1634) 1%	
	1760 (1714) 3%	2263 (2362) 4%	2766 (2783) 1%	3268 (3108) 5%		

The comparison of the predicted and measured tones for $\alpha = 0^\circ$ in Table 7 shows good agreement, with a greatest relative error being 5%. The primary tone at $Re = 50,000$ and $100,000$ was predicted within 1%. The primary tone at $Re = 150,000$ and $\alpha = 0^\circ$ was, however, not captured using this feedback model and is still under investigation.

Table 8. Feedback analysis at $\alpha = 1.58^\circ$, using the boundary layer separation feedback length, L . The predicted tones (Hz) using a feedback model are shown and the experimentally measured tones are presented in brackets. The relative error of the predicted to the experimentally measured tones is also presented. The primary tone is presented in bold case.

Re $\times 10^3$	n					
	3	4	5	6	7	8
50			520 (514) 1%	614 (605) 2%	709 (701) 1%	
			1493 (1471) 1%	1764 (1714) 3%		
	2535 (2678) 5%	3098 (2904) 7%	3662 (3377) 8%			

At $\alpha = 1.58^\circ$ good agreement is observed between the predicted and measured tones presented in Table 8. The greatest error for all of the Reynolds numbers considered was 8% and all of the primary tones were predicted within 7% of the measured tones.

Employing the point of maximum velocity on the airfoil surface as the feedback length L yielded greater errors (average >10%) for each of the primary and secondary tones. For some of the secondary tones, values of n were not able to be obtained to generate a valid comparison between the measured and predicted tones to within a 10% error.

A schematic diagram of the proposed feedback model based on the boundary layer separation feedback length is presented in Figure 13.

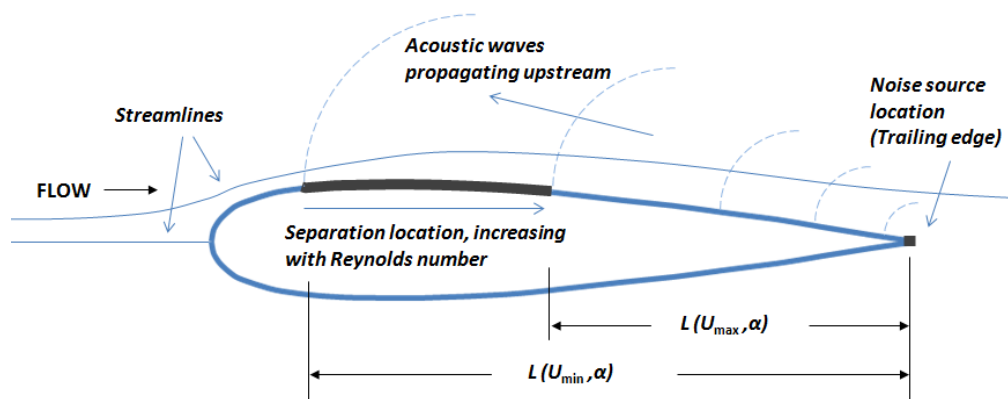


Figure 13. Schematic diagram of the proposed feedback model. The minimum and maximum feedback lengths are depicted to show the variation of the feedback length with Reynolds number and angle of attack. The schematic region of flow separation is identified as dark shading on the airfoil upper surface. The acoustic waves originate from the trailing edge and propagate upstream to a point of reinforcement, being the location of boundary layer separation, closing the feedback loop.

CONCLUSION

An acoustic feedback model using the distance between the boundary layer separation point and the trailing edge has been proposed to explain the generation of tonal noise from a NACA 0012 airfoil in low-to-moderate Reynolds number flows. Good agreement was achieved between the predicted tones using this model and experimentally obtained values.

Future work will involve the investigation of the effect of the airfoil suction side and its impact on the measured tonal noise and whether its contribution impacts the validity of the proposed feedback model.

REFERENCES

Amiet, R. 1977, *Refraction of Sound by a Shear Layer*, 15th AIAA Aeroacoustic Conference, AIAA 1977-54.

Arbey, H. and Bataille, J. 1983, *Noise generated by airfoil profiles placed in a uniform laminar flow*, Journal of Fluid Mechanics, Vol. 134.

Arcondoulis, E. J. G., Doolan C. J., Brooks L. A and Zander A. C., 2011, *A Modification to Logarithmic Spiral Beamforming Arrays for Aeroacoustic Applications*, 17th AIAA/CEAS Aeroacoustics Conference (32nd AIAA Aeroacoustics Conference), AIAA-2011-2720, June 6-8 2011, Portland, OR.

Arcondoulis, E.J.G., Doolan C.J., Brooks L.A and Zander A.C., 2012, *On the generation of airfoil tonal noise at zero angle of attack and low to moderate Reynolds number*, 18th AIAA/CEAS Aeroacoustics Conference (33rd AIAA Aeroacoustics Conference), AIAA-2012-2613, June 4-6 2012, Colorado Springs, CO.

Brooks, T., Pope D. and Marcolini, M. 1989, *Airfoil Self-Noise and Prediction*, Tech. rep., NASA Reference Publication 1218.

Brooks, T. F. and Humphreys, W. M. Jr. 2006, *A Deconvolution Approach for the Mapping of Acoustic Sources (DAMAS) determined from Phased Microphone Arrays*, Journal of Sound and Vibration, Vol. 294, pp. 856-879.

Desquesnes, G., Terracol, M. and Sagaut, P. 2007, *Numerical investigation of the tone noise mechanism over laminar airfoils*, Journal of Fluid Mechanics, Vol. 591, pp. 155-182.

Drela, M. 1989, *XFOIL: An analysis and design system for low Reynolds Number airfoils*, Conference on Low Reynolds Number Airfoil Aerodynamics, University of Notre Dame.

Ffowcs Williams, J. E. and Hall, L. H, 1970, *Aerodynamic Sound Generation by Turbulent Flow in the Vicinity of a Scattering Half Plane*, Journal of Fluid Mechanics. Vol. 40, pp. 657-670.

Lowson, M. V., Fiddes, S. P. and Nash, E. C. 1994, *Laminar Boundary Layer Aeroacoustic Instabilities*, 32nd Aerospace Sciences Meeting and Exhibition, AIAA 94-0358, 1994, Reno, NV.

Nash, E., Lowson, M. and McAlpine, A. 1998, *Boundary-Layer Instability Noise on Aerofoils*, Journal of Fluid Mechanics, Vol. 382, 1998, pp. 27-61.

Paterson, R., Vogt, P., Fink, M. and Munch, C. 1973, *Vortex Noise of Isolated Airfoils*, J.Aircraft, Vol. 10, No. 5.

Tam, C. 1974, *Discrete Tones of isolated airfoils*, The Journal of the Acoustic Society of America, Vol. 55, No.6.

Tam, C. and Ju, H. 2011, *Airfoil Tones at Moderate Reynolds Number: A Computational Study*, 17th AIAA/CEAS Aeroacoustics Conference (32nd AIAA Aeroacoustics Conference), AIAA-2011-2711, June 6-8 2011, Portland, OR.